Synthesis and characterization of transition metal complex cationed heptaborate structures

Ahmet Genç [1], **Dursun Ali Köse** [1,*], **Onur Şahin** [2]

[1]*Hitit University, Department of Chemistry, Ulukavak, Çorum, 19100, Türkiye*
[2]*Sinop University, Faculty of Health Sciences, Occupational Health And Safety Department, Sinop, 57000, Türkiye*

ARTICLE INFO

ABSTRACT

In recent years, interest in the study of cyclic borate structures (hexaborate, heptaborate, etc.), which draws attention due to their piezoelectric properties, has increased. In the scope of our study, heptaborate rings using the transition metal cation coordination compound as cation were synthesized and tried to be structurally characterized by elemental analysis, melting point determination, FT-IR, TGA/DTA analysis, UV analysis, powder x-ray diffraction (P-XRD) analysis methods. The presence of the cationic coordination sphere in the structures was determined by the stretching vibrations of ν(-M-N)$_{phen}$ and ν(-M-N)$_{pyrd}$ observed in the infrared spectra. -OH peaks of characteristic B-OH bonds of heptaborate rings and sharp asymmetric and symmetric stretching vibrations were detected confirming the presence of trigonal borate molecule in the rings. Due to the similar thermal decomposition properties of the molecules, it was determined that the hydrated waters that precipitated out of the coordination sphere in all structures moved away from the structures in a single step. As the second degradation step of heptaborate salt structures, the presence of water in amounts attributable to the removal of -OH groups in borate rings as water vapor in all structures was calculated. It has been observed that this degradation step occurs in a single step in all structures and the relevant experimental theoretical mass losses are compatible with each other. Combustion degradation of organic ligands was observed as the final degradation step of the heptaborate salt structures with metal cation complexes. While peaks belonging to heptaborate rings were observed from the recorded powder x-ray diffraction patterns, electronic transition data also supported that the metal cation complex was in octahedral geometry.

1. Introduction

Borates are mostly classified as hydrated metal borates or solvo mixed metaloxides. The structural features of only about 100 of the 200 borate minerals found are known [1,2]. Some synthesized borate structures reveal dissociated, cleaved borate or polyborate anions. However, most of them release condensed anions that form chains, layers and networks. In studies, it has been determined that the counter metal cations of boroxol (B_3O_3) are a structure that affects Lewis acidity at different levels. However, it has been determined that boric acid in borate structures is in a tetrahedral coordination position with strong Lewis acidic properties [2-6]. Boron-oxygen containing compounds have many uses in the industrial field due to various structural aspects. Polyborate-containing compounds are used in the manufacture of non-linear optical materials as well as luminescent materials and lithium electrode batteries. Due to their thermal properties, interest in studies on polyborate compounds in both industrial and academic fields

has increased [7-15]. Among the borate compounds obtained as a result of laboratory studies, there are also anionic pentaborate and hexaborate salts in the form of non-metallic structures with complementary cations. Structural characterizations of some of these borate structures without metal cations were made and $[B_3O_3(OH)_4]$, $[B_4O_5(OH)_4]^{2-}$, $[B_5O_6(OH)_4]$, $[B_7O_9(OH)_5]^{2-}$, $[B_9O_{12}(OH)_6]^{3-}$, $[B_{14}O_{20}(OH)_6]^{4-}$ and $[B_{15}O_{20}(OH)_8]^{3-}$ [16-19]. The chemical interaction tendencies of compounds with metal cations with borate anions are different from compounds without metal cations. Compared to spherical metal cations, non-spherical metal cation-free cationic compounds behave differently in terms of gaining electrons from the oxygen atom and making H-bonds [20,21]. Steric and electronic factors also significantly affect the structure of metal cation-free borate compounds. For example, while the metal cation-free borate structures, ammoniumboride $\{[NH_4]_3[B_{15}O_{20}(OH)_8].4H_2O\}$ and larderite $\{[NH_4][B_5O_7(OH)_2].H_2O\}$ have anionic borate structures paired with the ammonium cation. Polyborate systems

*Corresponding author: dalikose@hitit.edu.tr

obtained from compounds containing amine groups such as guanidinium and imidizolium are metal cation-free borate compounds containing $[B_9O_{12}(OH)_6]^{3-}$ nonaborate anion [2,13,22].

Two different borate compounds synthesized without metal cation $[(CH_3NH_3)_4][B_{14}O_{20}(OH)_6]$ and with metal cation $[Zn(en)_2[B_7O_{10}(OH)_3]$ are molecules constructed with different B_7 (heptaborate ring) species [23]. $[Cu(C_{12}H_8N_2)_2(C_2H_3O_2)][B_5O_6(OH)_4]\cdot 2H_3BO_3\cdot H_2O$ and $[Ni(C_{12}H_8N_2)_2(H_2O)_2]\cdot(B_7O_9(OH)$ synthesized as polyoxoborate and can be examples of pentaborate and heptaborate structures with metal cations formulated structures were characterized in another study [24].

Single crystals of three different oxidopolyborate salts with the formulas $[Co(NH_3)_6]_2[B_4O_5(OH)_4]_3\cdot 11H_2O$, $[Ni(phen)_3][B_7O_9(OH)_5]\cdot 9H_2O$ and $[Zn(dac)_2(H_2O)_2][B_7O_9(OH)_5]\cdot H_2O$ were formed, yielding anhydrous borate residues such as CoB_6O_{10}, NiB_7O_{11} and ZnB_7O_{11} by thermal decomposition and structural was scrutinized [25].

The properties of crystalline hydrated polyborate salt structures containing co-polyborate anions synthesized with cationic metal complexes or organic cations were investigated. The salt structures described by Clark, Christ, and Burns were studied between 2000 and 2015 and describe the synthesis approaches and physical and spectroscopic properties of polyborate salts with three different methods such as hydrothermal, solvothermal, and flow methods [26]. Metal borate halides containing halogen anions (F, Cl, Br or I) in their structures are also considered as high performance nonlinear optical (NLO) materials. Borate structures containing halogen anions form numerous metal borate halides in anionic structures ranging from 0D clusters, 1D chains, 2D layers and 3D meshes. NLO material properties are considered to be the most prominent features of cyclic borate anions [27].

In the present study, cyclic heptaborate anions were synthesized using their complex structures containing transition metal cations (Mn^{2+}, Co^{2+}, Ni^{2+}, Cu^{2+}, Zn^{2+} and Cd^{2+}) as stabilizing cations. The structures were characterized using elemental analysis, melting point determination, FT-IR, TGA/DTA analysis, Solid-state UV-vis spectroscopy, P-XRD methods.

2. Experimental Studies

2.1. Synthesis of Metal Heptaborate Structure

1 mmol metal acetate (Mn^{2+}, Co^{2+}, Ni^{2+}, Cu^{2+}, Zn^{2+} and Cd^{2+}) salts prepared in 50 mL aqueous solution were first mixed with 9 mmol boric acid solution with the one prepared in 50 mL water. 4 mmol of 1,10-phenanthroline and 4 mmol of pyridine ligands were added to the total solution, which was stirred on a magnetic stirrer for about 30 minutes, and the final solution was refluxed at 80°C on a heated magnetic stirrer for 72 hours. The complex solution, which was transferred to a beaker after reflux, was kept for 5 hours by adding distilled water on top of it to maintain the total solution amount, on a heated magnetic stirrer at 60°C, with continuous stirring to evaporate the acetic acid in the environment. After the sharp smell of acetic acid disappeared, the beaker was closed with parafilm and the final solution was allowed to crystallize. After approximately 30 days, the walls of the beaker and the crystals that precipitated adhered to the bottom of the beaker were filtered off with a vacuum system and stored for analysis (Figure 1).

2.2. Characterization Studies

C, H, N contents were determined by an CHNS-932 LECO model analytical instrument. Water contents were determined thermogravimetrically. Melting points were determined by an Electrothermal 9100 model instrument. Thermal analyses (TGA, DTA) were performed by the Shimadzu DTG-60H system, in dynamic nitrogen atmosphere (100 mL/min) at a heating rate of 10°C/min, in platinum crucibles as sample vessel, using -Al_2O_3 as reference. FTIR spectra were measured in the 450-4000 cm^{-1} range with a Perkin-Elmer Spectrum One instrument by using the KBr pellet technique. Powder x-ray diffraction patterns were recorded with the Rigaku Ultima-IV model device. For solid state UV-vis visible region spectra, solid state UV-Vis studies were carried out in the range of 200-900 nm with Schimadzu brand UV-3600 UV-VIS NIR Spectrophotometer device. Magnetic susceptibility measurements were determined on the Sherwood Scientific MXI model magnetic balance (Gouy Method) using the $Hg[Co(SCN)_4]$ reference at room temperature.
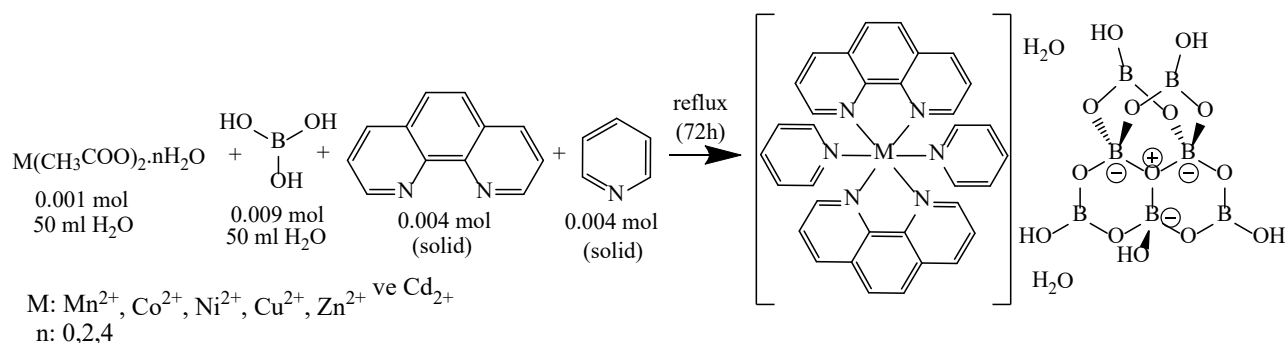

Figure 1. Synthesis reaction of heptaborate structures with metal complex cations.

3. Characterisation

3.1. Elemental Analysis

Chemical composition analyzes of heptaborate salt structures of synthesized transition metal cation complexes were carried out. In addition, magnetic susceptibility and melting point values in Bohr magnetons were determined in order to determine the transition metal-based magnetic properties of metal cation complexes and to determine the number of single-electron orbitals they contain in their final orbits. The suitability of experimental and theoretical results supports the accuracy of the proposed molecular formulas. The results obtained are given in Table 1. It is thought that some deviations in the values are caused by organic and inorganic residues attached to the structure while heptaborate salts are synthesized. According to stoichiometric mole ratios, the maximum amount of substance that can be obtained with the starting materials was accepted as 100% theoretical yield and the % yield calculations were carried out for each synthesis by proportioning it with the actual yield obtained experimentally from the reactions. In addition, according to these values, we can say that while the molecule with the highest efficiency is the heptaborate salt structure containing the zinc complex, compound **V** with 68%, the compound with the lowest efficiency is the heptaborate salt containing the cadmium complex, the molecule **VI** with 52%.

The heptaborate salt with the highest melting point at 229°C is the heptaborate salt with Co(II) metal cation complex, compound no. **II**, while the pentaborate salt with the lowest melting point is the Ni(II) metal cation, compound no. **III**, at 130°C. complex heptaborate salt.

3.2. Infrared Analysis

The FT-IR spectra of heptaborate salt structures of manganese, cobalt, nickel, copper, zinc and cadmium cation complexes containing neutral 1,10-phenanthroline and pyridine ligands are given in Figure 2. It is confirmed that the infrared spectra are also very similar due to the similarity of the structural properties of the molecules. Some important bond stress bending vibrations of heptaborate salt molecules are also summarized in Table 2. The -OH stretching vibrations, which are generally thought to originate from the hydrated water in the structures, appear as a broad and wide peak between 3600-3550 cm^{-1} and 2900 cm^{-1}. It was observed that the -OH stretching vibrations of the B-OH bond in the heptaborate structure appeared as sharp peaks in the
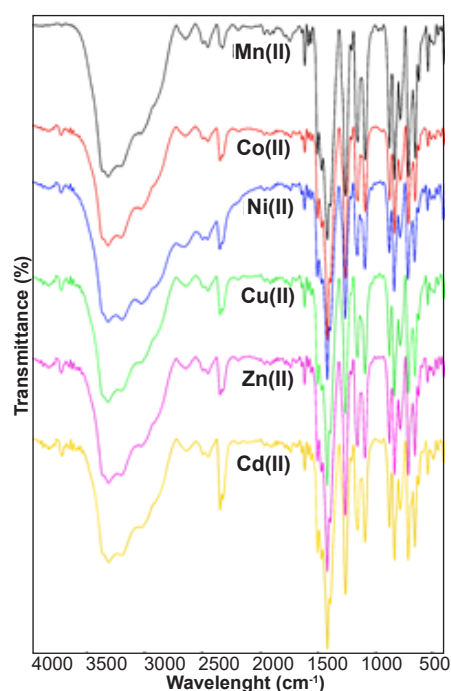

Figure 2. Infrared spectra of heptaborate structures with transition metal complex cations.

Table 1. Significant infrared peaks of heptaborate structures with transition metal complex cations.

| Complexes | MW (g/mol) | Yield (%) | Chemical Analysis (%) | | | Colour | μ_{eff} | Decomp. Temp. (°C) |
| | | | Exp. | (Theo.) | | | | |
			C	H	N			
[Mn(C₁₂H₈N₂)₂(C₅H₅N)₂](B₇O₉(OH)₅).2H₂O $C_{34}H_{35}B_7MnN_6O_{16}$ (I)	914.29	58	44.97 (44.63)	3.45 (3.83)	9.24 (9.19)	Pale white	4.77	218
[Co(C₁₂H₈N₂)₂(C₅H₅N)₂](B₇O₉(OH)₅).2H₂O $C_{34}H_{35}B_7CoN_6O_{16}$ (II)	918.28	61	44.72 (44.43)	3.32 (3.81)	9.10 (9.15)	Orange	3.16	229
[Ni(C₁₂H₈N₂)₂(C₅H₅N)₂](B₇O₉(OH)₅).2H₂O $C_{34}H_{35}B_7N_6NiO_{16}$ (III)	918.04	59	44.95 (44.44)	3.27 (3.81)	9.09 (9.15)	Lilac	2.13	130
[Cu(C₁₂H₈N₂)₂(C₅H₅N)₂](B₇O₉(OH)₅).2H₂O $C_{34}H_{35}B_7CuN_6O_{16}$ (IV)	922.90	62	43.94 (44.21)	4.12 (3.79)	9.03 (9.10	Light blue	1.39	219
[Zn(C₁₂H₈N₂)₂(C₅H₅N)₂](B₇O₉(OH)₅).2H₂O $C_{34}H_{35}B_7N_6O_{16}Zn$ (V)	924.73	68	43.87 (44.12)	4.19 (3.79)	9.16 (9.09)	Light yellow	dia.	221
[Cd(C₁₂H₈N₂)₂(C₅H₅N)₂](B₇O₉(OH)₅).2H₂O $C_{34}H_{35}B_7CdN_6O_{16}$ (VI)	971.76	52	41.62 (41.99)	3.93 (3.60)	8.71 (8.65)	Pale pink	dia.	217

region of approximately 3334-3331 cm^{-1}.

ν(C=N) stretching vibrations, which can be attributed to the 1,10-phenanthroline and pyridine ligands in the structure of metal cation complexes that serve as the stabilizing cations of the molecules, were observed at approximately 2360-2357 cm^{-1} and 2337-2331 cm^{-1} regions for all structures, respectively. In addition, stretching vibrations ν(C=C) of aromatic rings of organic ligands were also observed as multiple peaks of moderate and weak intensity in the range of 1753-1745 cm^{-1} and 1478-1453 cm^{-1}. Bending vibrations of ν(C=C) and ν(C-C) aromatic rings showed themselves in the range of 887-665 cm^{-1} as medium and high intensity sharp peaks. Asymmetric and symmetric stretching vibrations ν(-B-O)$_{BO3asym}$ and ν(-B-O)$_{BO3sym}$, proving the existence of four trigonal borate molecules in the heptaborate ring structure, in the 1427-1426 cm^{-1} and 1403-1402 cm^{-1} regions for all heptaborate structures, respectively, observed as sharp peaks. Asymmetric and symmetrical ν(-B-O)$_{BO4asym}$ ve ν(-B-O)$_{BO4sym}$ stretching vibrations, which can be attributed to the anionic three tetrahedral borate structures in the heptaborate ring structure, were also detected at approximately 1166-1164 cm^{-1} and 1099-1098 cm^{-1} regions. The fact that the stress vibrations attributed to the trigonal and tetragonal ν(-B-O) groups in all metal cation complexes are close to each other supports that the polyborate derivative in all structures has the same structure.

In addition, the stretching vibration of the B-O bond is expected to be observed in the range of 1380-1310 cm^{-1} in non-polyborate boroxide compounds [14,17,28,29]. However, in polyborate derivatives (pentaborate, hexaborate or heptaborate) where B-O-B bonding is prominent, the stretching peak of this bonding has been determined to shift up to the range of 1270-1220 cm^{-1} [18,19]. In the synthesized heptaborate molecules, the stretching vibration attributable to this binding was observed to be around 1271-1269 cm^{-1} for all structures. Stretching vibrations indicating the bindings that may indicate the presence of metal-ligand bonding, which forms the structure of

metal cation complexes, were also observed in the ν(-M-N)$_{phen}$ region of approximately 555-552 cm^{-1} for the bidentate ligand 1,10-phenanthroline. For the monodentate coordinated pyridine ligand, ν(-M-N)$_{pyrd}$ appeared at approximately 504-493 cm^{-1} regions.

3.3. Thermal Analysis

The thermal degradation diagrams of heptaborate salt structures are shown in Figure 3, and the data summarizing the degradation steps formed from the thermal analysis curves are summed up in Table 3.

The thermal degradation diagrams of heptaborate structures with cation metal complexes are similar depending on their iso-structure properties. For all structures, thermal decompositions begin with the separation of two hydrated waters, which are outside the coordination ring and related to the main structure by Vander-Wals interactions. After this degradation stage, which takes place in the range of approximately 56-130 °C, the second decomposition step, in which the heptaborate ring dehydrates, takes place. For all structures, the -OH groups of heptaborate rings are thought to be removed in the decomposition that takes place in the temperature regions of 126-175 °C and indicates the removal of 5/2 units of H$_2$O. The compatibility of the experimental and theoretical weight loss calculations in all structures supports the relevant degradation product. As the final degradation step of heptaborate structures, the degradation of organic ligands of the cationic metal complex can be shown. It has been determined that this degradation step generally starts at 150°C levels and ends at 955°C levels for all structures. The organic ligands 1,10-phenanthroline and pyridine derivatives burned away from the structures in the respective degradation step, and it was interpreted that the experimental and theoretical weight loss amounts were compatible. It was approved by powder x-ray diffraction analysis that oxides of the respective metal cations and residues of boron oxide remained in the reaction cup as final degradation products of heptaborate salt structures. The fact that the theoretical residue calculations for

Table 2. Significant infrared peaks of heptaborate structures with transition metal complex cations.

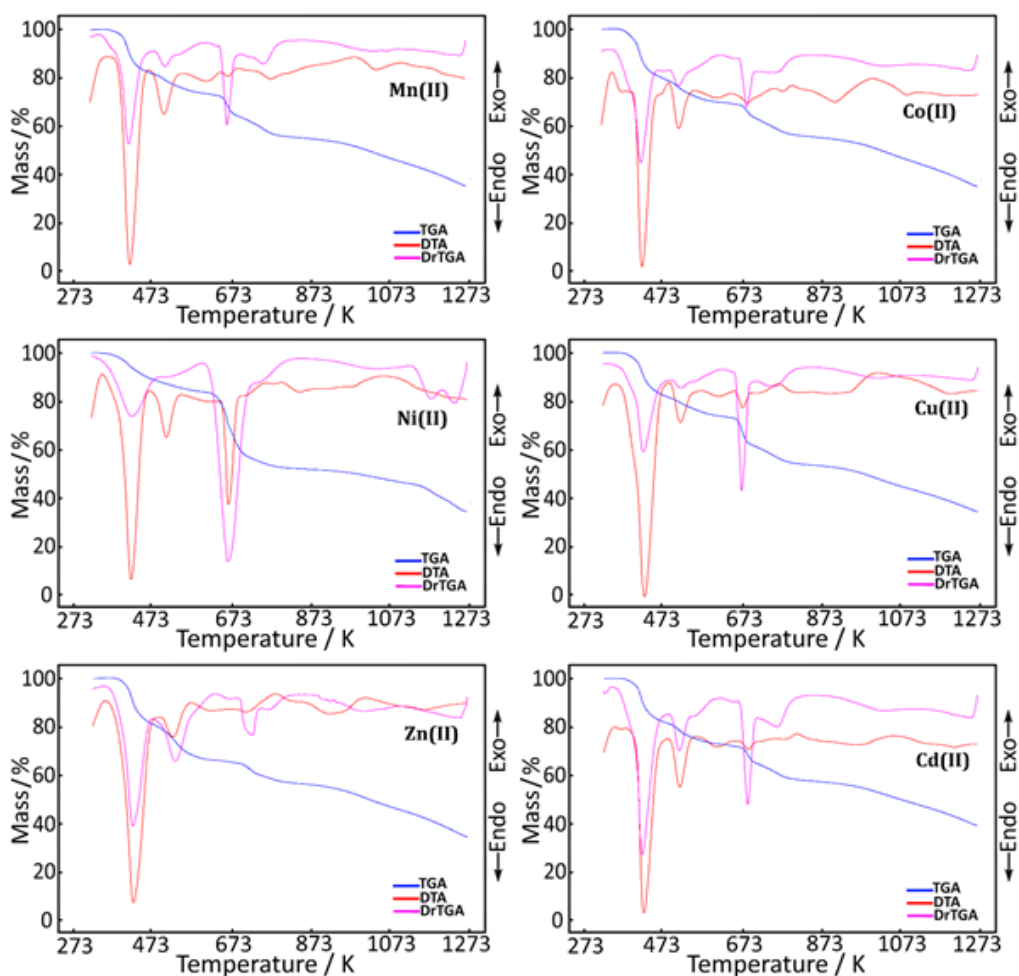| Gruplar	Mn(II)	Co(II)	Ni(II)	IV	V	VI
ν(-OH)$_{H2O}$	3550-2900	3550-2900	3550-2900	3500-2900	3600-2900	3600-2900
ν(-OH)$_{B-OH}$	3332	3332	3332	3334	3331	3332
ν(C=N)$_{phen,pyrd}$	2357;2337	2360;2335	2360;2331	2360;2332	2359;2332	2360;2334
ν(C=C)$_{phen,pyrd}$	1753-1478	1749-1477	1745-1473	1747-1477	1747-1478	1750-1478
ν(-B-O)$_{BO3asym}$	1427	1426	1426	1426	1427	1427
ν(-B-O)$_{BO3sym}$	1402	1402	1403	1402	1402	1402
ν(-B-O)$_{BO4asym}$	1165	1166	1165	1165	1165	1164
ν(-B-O)$_{BO4sym}$	1099	1099	1099	1098	1099	1098
ν(-B-O-B)	1270	1271	1270	1269	1270	1270
δ(C=C); (C-C)	887-665	887-666	886-666	886-664	887-665	886-665
ν(-M-N)$_{phen}$	553	555	553	552	554	552
ν(-M-N)$_{pyrd}$	504	493	493	496	502	503

Figure 3. Thermal analysis curves of heptaborate structures with transition metal complex cations..

metal oxides are compatible with the experimental results also supports our claim. It has been determined that the experimental residue amounts are approximately 1% higher than the theoretical amounts. The reason for this is thought to be due to the incomplete combustion of the organic derivatives in the structures due to insufficient oxygen, thermal decomposition curves recorded in the inert nitrogen environment. The carbonized carbon, which could not burn completely and accumulated on the oxide residues, also caused the colors of all oxides to be black.

3.4. X-Ray Analysis

In Figure 4, P-XRD patterns of heptaborate salt structures using transition metal cation (Mn^{2+}, Co^{2+}, Ni^{2+}, Cu^{2+}, Zn^{2+} and Cd^{2+}) complexes as stabilizing ions are given. It was stated that all of the molecules, which were tried to obtain information about their structural characterization by powder x-ray diffraction method, were in crystalline structure, but crystals suitable for single crystal structure analysis studies could not be collected. The peaks marked with an "X" in the patterns indicate the formation of heptaborate rings [30]. According to the recorded P-XRD patterns, it can be said that the heptaborate salt with the Cd(II)

metal cation-centered complex structure has the best crystallinity, while the heptaborate salt with the Zn(II) metal cation-centered complex structure has the weakest crystallinity.
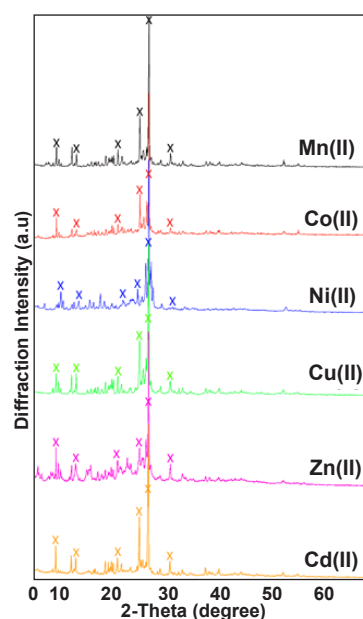

Figure 4. GP-XRD patterns of heptaborate structures with transition metal complex cations.

Table 3. Decomposition steps and degradation product details obtained by calculating from thermal analysis curves of complex structures.

Compound	Step	Temperature Range (K)	DTA$_{max}$	Removed Group	Mass Loss (%) Exp.	Mass Loss (%) Calc.	Remained Product (%) Exp.	Remained Product (%) Calc.	Decomp. Product	Colour
[Mn(C$_{12}$H$_8$N$_2$)$_2$(C$_5$H$_5$N)$_2$](B$_7$O$_9$(OH)$_5$)·2H$_2$O C$_{34}$H$_{35}$B$_7$MnN$_6$O$_{16}$ 914.29 g/mol	1	73-130	94	2H$_2$O	3.71	(3.94)				Pale-yellow
	2	132-160	139	5/2H$_2$O	5.62	(4.92)				
	3	161-955	227;335;389;-468;-721	2C$_{12}$H$_8$N$_2$;2C$_5$H$_5$N	54.75	(56.72)	35.92	(34.56)	MnO;7/2B$_2$O$_3$	Black
[Co(C$_{12}$H$_8$N$_2$)$_2$(C$_5$H$_5$N)$_2$](B$_7$O$_9$(OH)$_5$)·2H$_2$O C$_{34}$H$_{35}$B$_7$CoN$_6$O$_{16}$ 918.28 g/mol	1	61-121	86	2H$_2$O	3.86	(3.92)				Brick-color
	2	123-155	137	5/2H$_2$O	5.78	(4.90)				
	3	156-955	233;330;407;-523;-731	2C$_{12}$H$_8$N$_2$;2C$_5$H$_5$N	54.63	(56.48)	35.73	(34.84)	CoO;7/2B$_2$O$_3$	Black
[Ni(C$_{12}$H$_8$N$_2$)(C$_5$H$_5$N)$_2$](B$_7$O$_9$(OH)$_5$)·2H$_2$O C$_{34}$H$_{35}$B$_7$N$_6$NiO$_{16}$ 918.04 g/mol	1	56-125	85	2H$_2$O	3.92	(3.92)				Light-green
	2	126-175	133	5/2H$_2$O	4.71	(4.90)				
	3	177-955	224;329;386;-523;-790	2C$_{12}$H$_8$N$_2$;2C$_5$H$_5$N	55.39	(56.49)	35.98	(34.82)	NiO;7/2B$_2$O$_3$	Black
[Cu(C$_{12}$H$_8$N$_2$)$_2$(C$_5$H$_5$N)$_2$](B$_7$O$_9$(OH)$_5$)·2H$_2$O C$_{34}$H$_{35}$B$_7$CuN$_6$O$_{16}$ 922.90 g/mol	1	63-124	98	2H$_2$O	3.49	(3.90)				Blue
	2	125-154	137	5/2H$_2$O	5.35	(4.88)				
	3	156-955	228;328;391;-485;-743	2C$_{12}$H$_8$N$_2$;2C$_5$H$_5$N	54.75	(56.20)	36.47	(35.17)	CuO;7/2B$_2$O$_3$	Black
[Zn(C$_{12}$H$_8$N$_2$)$_2$(C$_5$H$_5$N)$_2$](B$_7$O$_9$(OH)$_5$)·2H$_2$O C$_{34}$H$_{35}$B$_7$N$_6$O$_{16}$Zn 924.73 g/mol	1	59-123	94	2H$_2$O	3.60	(3.89)				White
	2	124-151	133	5/2H$_2$O	6.02	(4.87)				
	3	153-955	237;338;426;-504;-733	2C$_{12}$H$_8$N$_2$;2C$_5$H$_5$N	53.76	(56.08)	36.62	(35.30)	ZnO;7/2B$_2$O$_3$	Black
[Cd(C$_{12}$H$_8$N$_2$)$_2$(C$_5$H$_5$N)$_2$](B$_7$O$_9$(OH)$_5$)·2H$_2$O C$_{34}$H$_{35}$B$_7$CdN$_6$O$_{16}$ 971.76 g/mol	1	72-124	91	2H$_2$O	3.58	(3.70)				Plae-white
	2	126-164	136	5/2H$_2$O	5.02	(4.63)				
	3	166-955	229;324;405;-533;-781	2C$_{12}$H$_8$N$_2$;2C$_5$H$_5$N	51.28	(53.37)	40.12	(38.43)	CdO;7/2B$_2$O$_3$	Black

3.5. Ultraviolet-Visible Spectroscopy

The visible region spectra (UV-vis) recorded in solid phase in the range of 900-200 nm of heptaborate anion salt structures using synthesized transition metal cation (Mn^{2+}, Co^{2+}, Ni^{2+}, Cu^{2+}, Zn^{2+} ve Cd^{2+}) complexes as stabilizing ions are shown in Figure 5.
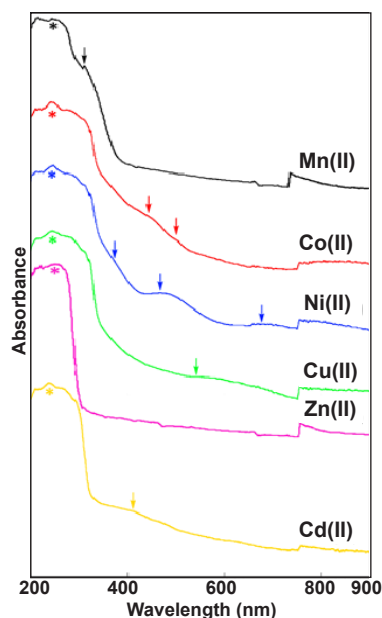

Figure 5. Solid state UV-vis spectra of heptaborate structures with transition metal complex cations.

Significant peak values and electronic transition values are also summarized in Table 4. According to these data, the d-d transitions attributable to the Mn(II) metal cation complex (**I**) occur at 303 nm ($^4T_{1g}{\rightarrow}^4T_{2g}$) (F). For the electronic transitions of the Co(II) metal cation complex (**II**), two spin-permitted d-d transitions were observed at 493 nm ($^4T_{1g}{\rightarrow}^4T_{2g}$)(F) and 426 nm ($^4T_{1g}{\rightarrow}^4T_{2g}$)(P). For the complex (**III**) cation using the Ni(II) metal cation as the central atom, 678 nm for the ($^3A_{2g}{\rightarrow}^3T_{1g}$)(P) transition, 462 nm for the ($^3A_{2g}{\rightarrow}^3T_{1g}$) (F) transition, and $^3A_{2g}{\rightarrow}^3T_{2g}$)(F) For the) transition, a total of three spin-permitted electronic transitions at 381 nm wavelengths were detected. For the complex cation (III) using Ni(II) metal cation as the central

atom, 678 nm for the ($^3A_{2g}{\rightarrow}^3T_{1g}$)(P) transition, 462 nm for the ($^3A_{2g}{\rightarrow}^3T_{1g}$)(F) transition, and 381 nm for the ($^3A_{2g}{\rightarrow}^3T_{2g}$)(F) transition, total of three spin-permitted electronic transitions were detected. These transitions confirm that the "*d*" orbitals of the Ni(II) metal cation are cleaved, indicating the octahedral geometry. The multi-absorption bands of the Cu(II) metal cation structure (**IV**) are composed of overlapping peaks and have a broad appearance in a wide range, and it is seen that they coincide with the 730-420 nm range. These spectral data support the view that the Cu^{2+} metal cation may have a "*pseudo-octahedral*" structure with the effect of Jahn-Teller decomposition. The maximum absorption band of the broad spectrum of the Cu(II) complex also corresponds to a wavelength of approximately 531 nm ($^2E_g{\rightarrow}^2T_{2g}$). Since the d orbitals in the last orbit of the metal cation in the diamagnetic Zn(II) complex (V) are fully occupied, the "*d-d*" electronic transition could not be detected in the octahedral cleavage. Magnetic susceptibility values confirm this situation. As it can be understood from the magnetic susceptibility values, no "*d-d*" electronic transition could be detected in an octahedral cleavage that may occur because the d orbitals in the last orbit of the metal cation in the complex (**V**) with the diamagnetic Zn(II) metal cation are fully filled. Again, no "*d-d*" electronic transition is expected in an octahedral cleavage due to the fact that the "*d*" orbitals in the last orbit are fully occupied in the metal cation in the complex (**VI**) structure with Cd(II) metal cation, which we can evaluate as diamagnetic according to the magnetic susceptibility values. However, electronic transitions at 401 nm ($^2E_g{\rightarrow}^2T_{2g}$) have been detected, albeit weakly, in the low region due to the orbital interferences of the Cd(II) metal cation, which is also consistent with the literature [31-33]. It is predicted that the absorption bands seen at low wavelength with high intensity do not belong to "*d-d*" transitions, but may result from metal → ligand charge transfer transitions with stronger energy. These transitions are 242 nm for complex **I**, 241 nm for complex **II**, 245 nm for complex **III**, and 245 nm for complex **IV**. While the absorption bands at wavelengths belong to metal → ligand (M→L) transitions, the intense peaks observed at 231 nm for complex IV and 234 nm for complex IV are ligand → metal (L→M) are considered to belong to the charge transfer bands.

Table 4. UV-Vis spectra of metal-coumarilate mixed ligand complexes.

Transitions	Mn(II) (oktahedral)	Co(II) (oktahedral)	Ni(II) (oktahedral)	Cu(II) (oktahedral)	Zn(II) (oktahedral)	Cd(II) (oktahedral)
d-d	303 ($^4T_{1g}{\rightarrow}^4T_{2g}$)(F)	493 ($^4T_{1g}{\rightarrow}^4T_{2g}$)(F)	678 ($^3T_{1g}{\rightarrow}^3T_{2g}$)(P)	730-420 531 ($^2E_g{\rightarrow}^2T_{2g}$)	–	401 ($^2Eg{\rightarrow}^2T_{2g}$)
d-d	–	426 ($^4T_{1g}{\rightarrow}^4T_{2g}$)(P)	462 ($^3T_{1g}{\rightarrow}^3T_{2g}$)(F)	–	–	–
	–	–	381 ($^3T_{1g}{\rightarrow}^3T_{2g}$)(F)	–	–	-
M→ L	242	241	245	245	–	-
L→M	–	–	–	–	231	234

4. Conclusions

Infrared spectra of heptaborate salt structures have confirmed the peaks of $\nu\text{(-M-N)}_{phen}$ and $\nu\text{(-M-N)}_{pyrd}$ stretching vibrations, which indicate the presence of a transition metal complex. As the characteristic stretching vibrations of the heptaborate structure, the -OH stretching vibrations of the B-OH bonds present in the structures and the asymmetric and symmetrical ν (-B-O)BO_{3asym} and $\nu\text{(-B-O)BO}_{3sym}$ stretching vibrations, which confirm the presence of four trigonal borate molecules in the structures, appear as sharp peaks. have been found out. At the same time, asymmetric and symmetrical $\nu\text{(-B-O)}_{BO4asym}$ and $\nu\text{(-B-O)}_{BO4sym}$ stretching vibrations, which can be attributed to the anionic three tetrahedral borate structures in the heptaborate rings, are also detected, and the tension vibrations that can be attributed to the trigonal and tetragonal ν(-B-O) groups are close to each other. supports that the polyborate derivative in all structures is similar in structure. Data on thermal decomposition steps and decomposition products were collected from thermal analysis curves showing similar decomposition properties. It is thought that thermal decompositions begin with the removal of the hydrate waters settled outside the coordination sphere from the structures in a single step and continue with the removal of -OH groups in the heptaborate rings in the form of water vapor. It is claimed that the organic ligands of the metal complex burn away from the structure as the final degradation step. The resulting powder was supported by P-XRD data, in which black colored residues of the corresponding metal oxide / boron oxide remained in all of the reaction vessels as the final degradation product of heptaborate compounds. From the electronic transitions of metal cations, it was determined that they have an octahedral coordination geometry in the 2+ charge order.

Acknowledgements

References

[1]. Schubert, D. M. (2003). Borates in Industrial Use. In H. W., Roesky, & D. A., Atwood (Eds.). *Group 13 Chemistry III. Structure and Bonding* (Vol. 105, pp. 1-40). Springer. https://doi.org/10.1007/3-540-46110-8_1.

[2]. Beckett, M. A., Bland, C. C., Horton, P. N., Hursthouse, M. B., & Varma, K. S. (2007). Supramolecular structures containing 'isolated' pentaborate anions and non-metal cations: Crystal structures of [Me3NCH2CH2OH][B5O6(OH)4] and [4-MepyH,4-Mepy][B5O6(OH)4]. *Journal of Organometallic Chemistry*, *692*(13), 2832-2838. https://doi.org/10.1016/j.jorganchem.2007.02.038.

[3]. Brown, I. D., O'Keeffe, M., & Navrotsky, A. (1981). *Structure and Bonding in Crystals*. Academic Press. https://doi.org/10.1016/B978-0-12-525101-3.X5001-3.

[4]. Schindler, M., & Hawthorne, F. C. (2001). A bond-valence approach to the structure, chemistry and paragenesis of hydroxy-hydrated oxysalt minerals. I. Theory. *Canadian Mineralogist*, *39*(5), 1225-1242. https://doi.org/10.2113/gscanmin.39.5.1225.

[5]. Schindler, M., & Hawthorne, F. C. (2001). A bond-valence approach to the structure, chemistry and paragenesis of hydroxy-hydrated oxysalt minerals. II. Crystal structure and chemical composition of borate minerals. *Canadian Mineralogist*, *39*(5), 1243-1256. https://doi.org/10.2113/gscanmin.39.5.1243.

[6]. Schindler, M., & Hawthorne, F. C. (2001). A bond-valence approach to the structure, chemistry and paragenesis of hydroxy-hydrated oxysalt minerals. III. Paragenesis of borate minerals. *Canadian Mineralogist*, *39*(5), 1257-1274. https://doi.org/10.2113/gscanmin.39.5.1257.

[7]. Cook Jr., W. R., & Jaffe H. (1957). The crystallographic, elastic and piezoelectric properties of ammonium pentaborate and potassium pentaborate. *Acta Crystallographica*. *10*, 705-707. https://doi.org/10.1107/S0365110X57002431.

[8]. Touboul, M., & Betourne, E. (1993). LiB2O3(OH)·H2O as precursor of lithium boron oxide LiB2O3.5: Synthesis and dehydration process. *Solid State Ionics*, *63-65*, 340-345. https://doi.org/10.1016/0167-2738(93)90126-N.

[9]. Akella, A., & Keszler, D. A. (1995). Structure and Eu2+ luminescence of dibarium magnesium orthoborate. *Materials Research Bulletin*, *30*(1), 105-111. https://doi.org/10.1016/0025-5408(94)00113-8.

[10]. Dotsenko, V. P., Efryushina, N. P., & Berezovskaya, I. V. (1996). Luminescence properties of GaBO3:Bi3+. *Materials Letters*, *28*(4-6), 517-520. https://doi.org/10.1016/0167-577X(96)00114-0

[11]. Soler-Illia, G. J. D. A., Sanchez, C., Lebeau, B., & Patarin, J. (2002). Chemical strategies to design textured materials: from microporous and mesoporous oxides to nanonetworks and hierarchical structures. *Chemical Reviews*, *102*(11), 4093-4138. https://doi.org/10.1021/cr0200062.

[12]. Yang, S., Li, G., Tian, S., Liao, F., & Lin, J. (2007). Synthesis and structure of [C2H10N2][B5O8(OH)]: A nonmetal pentaborate with nonlinear optical properties. *Crystal Growth & Design*, *7*(7), 1246-1250. https://doi.org/10.1021/cg0606794.

[13]. Liu, H. X., Liang, Y. X., & Jiang, X. (2008). Synthesis, crystal structure and NLO property of a nonmetal pentaborate [C6H13N2][B5O6 (OH) 4]. *Journal of Solid State Chemistry*, *181*(12), 3243-3247. https://doi.org/10.1016/j.jssc.2008.07.020.

[14]. Sızır, Ü., Yurdakul, Ö., Köse, D. A., & Akkurt, F. (2019). Novel non-metal cation (NMC) pentaborate salts of some amino acids. *Molecules*, *24*(15), 2790. https://doi.org/10.3390/molecules24152790.

[15]. Liu, W. F., Su, Z. M., Jia, Z., & Yang, G. Y. (2019). Syntheses, structures and characterizations of two new polyborates containing heptaborate sub-clusters. *Journal of Cluster Science*, *30*(4), 1139-1144. https://doi.org/10.1007/s10876-019-01577-w.

[16]. Merlino, S., & Sartori, F. (1971). Ammonioborite: New

borate polyion and its structure. *Science*, *171*(3969), 377-379. https://doi.org/10.1126/science.171.3969.377.

[17]. Schubert, D. M., Visi, M. Z., Khan, S., & Knobler, C. B. (2008). Synthesis and structure of a new heptaborate oxoanion isomer: B7O9(OH)52-. *Inorganic Chemistry*, *47*(11), 4740-4745. https://doi.org/10.1021/ic800068t.

[18]. Beckett, M. A., Horton, P. N., Coles, S. J., Kose, D. A., & Kreuziger, A. M. (2012). Structural and thermal studies of non-metal cation pentaborate salts with cations derived from 1, 5-diazobicyclo [4.3.0]non-5-ene, 1, 8-diazobicyclo [5.4.0]undec-7-ene and 1, 8-bis (dimethylamino) naphthalene. *Polyhedron*, *38*(1), 157-161. https://doi.org/10.1016/j.poly.2012.02.031.

[19]. Sızır, Ü., Yurdakul, Ö., Köse, D. A., & Içten, O. (2020). Zwitterionic amino acids as precursors for nonmetal cation pentaborate salts. *Journal of the Chinese Chemical Society*, *67*(10), 1849-1855. https://doi.org/10.1002/jccs.202000056.

[20]. Schubert, D. M., Smith, R. A., Visi, M. Z. (2003). Studies of crystalline nonmetal borates. *Glass Technology*, *44*(2), 63-70. Retrieved from https://www.ingentaconnect.com/content/sgt/gt/2003/00000044/00000002/art00006#trendmd-suggestions.

[21]. Köse, D. A., Beckett, M. A., Çolak, N. (2012). Synthesis, spectroscopic and thermal characterization of non-metal cation (nmc) pentaborates salts containing cations derived from histidine and arginine. *Hacettepe Journal of Biology and Chemistry*, *40*(3), 219-225. Retrieved from https://dergipark.org.tr/en/pub/hjbc/issue/61882/926041.

[22]. Schubert, D. M., Visi, M. Z., Knobler, C. B. (2000). Guanidinium and ımidazolium borates containing the first examples of an ısolated nonaborate oxoanion: [B9O12(OH)6]3-. *Inorganic Chemistry*, *39*(11), 2250-2251. https://doi.org/10.1021/ic000217u.

[23]. Yang, S., Li, G., Tian, S., Liao, F., & Lin, J. (2007). Synthesis and structure of [C2H10N2][B5O8(OH)]: a nonmetal pentaborate with nonlinear optical properties. *Crystal Growth & Design*, *7*(7), 1246-1250. https://doi.org/10.1021/cg0606794.

[24]. Köse, D. A., Yurdakul, Ö., Şahin, O., & Öztürk, Z. (2017). The new metal complex templated polyoxoborate(s) (POB(s)) structures. Synthesis, structural characterization, and hydrogen storage capacities. *Journal of Molecular Structure*, *1134*, 806-813. https://doi.org/10.1016/j.molstruc.2017.01.010.

[25]. Altahan, M. A., Beckett, M. A., Coles, S. J., & Horton, P. N. (2020). Oxidopolyborate anions templated by transition-metal complex cations: Self-assembled syntheses and structural studies (XRD) of [Co(NH3)6]2[B4O5(OH)4]3·11H2O, [Ni(phen)3][B7O9(OH)5].5H2O and [Zn(dac)2(H2O)2][B7O9(OH)5]·H2O. *Journal of Molecular Structure*, *1200*, 127071. https://doi.org/10.1016/j.molstruc.2019.127071.

[26]. Beckett, M. A. (2016). c. *Coordination Chemistry Reviews*, 323, 2-14.

[27]. Wang, Y., & Pan, S. (2016). Recent development of metal borate halides: Crystal chemistry and application in second-order NLO materials. *Coordination Chemistry Reviews*, *323*, 15-35. https://doi.org/10.1016/j.ccr.2015.12.008.

[28]. Liu, Z. H., & Li, L. Q. (2006). A new hydrated cesium heptaborate Cs2 [B7O9 (OH)5]: Synthesis and crystal structure. *Crystal Growth & Design*, *6*(6), 1247-1249. https://doi.org/10.1021/cg0503200.

[29]. Altahan, M. A., Beckett, M. A., Coles, S. J., & Horton, P. N. (2015). A new polyborate anion, [B7O9(OH)6]3−: Self assembly, XRD and thermal properties of s-fac-[Co(dien)2][B7O9(OH)6]· 9H2O. *Inorganic Chemistry Communications*, *59*, 95-98. https://doi.org/10.1016/j.inoche.2015.07.011.

[30]. Munirathnam, B., & Madhavan, J. (2009). Investigations on the structural, mechanical and photoconductive studies of pure and lanthanum doped potassium pentaborate single crystals. *Indian Journal of Science and Technology*, *2*(2), 44-45. https://doi.org/10.17485/ijst/2009/v2i2.8.

[31]. Chen, C. A., Pan, R., & Yang, G. Y. (2020). Syntheses and structures of a new 2D layered borate and a novel 3D porous-layered aluminoborate. *Dalton Transactions*, *49*(12), 3750-3757. https://doi.org/10.1039/C9DT03846A.

[32]. Huang, J. H., Jin, C. C., Xu, P. L., Gong, P., Lin, Z., Cheng, J. W., & Yang, G. Y. (2019). Li2CsB7O10(OH)4: A deep-ultraviolet nonlinear-optical mixed-alkaline borate constructed by unusual heptaborate anions. *Inorganic Chemistry*, *58*(3), 1755-1758. https://doi.org/10.1021/acs.inorgchem.8b03495.

[33]. Xu, C., Hedin, N., Shi, H. T., & Zhang, Q. F. (2014). A semiconducting microporous framework of Cd 6 Ag 4 (SPh) 16 clusters interlinked using rigid and conjugated bipyridines. *Chemical Communications*, *50*(28), 3710-3712. https://doi.org/10.1039/C3CC49660K.z.